Present wave climate in the Bay of Biscay: spatiotemporal variability and trends from 1958 to 2001

Elodie Charles, Déborah Idier, Jérôme Thiebot, Gonéri Le Cozannet, Rodrigo Pedreros, Fabrice Ardhuin, Serge Planton

Present Wave Climate in the Bay of Biscay: Spatiotemporal Variability and Trends from 1958 to 2001

ELODIE CHARLES, DÉBORAH IDIER, JÉRÔME THIÉBOT, GONÉRI LE COZANNET, AND RODRIGO PEDREROS

BRGM, Orléans, France

FABRICE ARDHUIN

Ifremer, Plouzané, France

SERGE PLANTON

Centre National de Recherches Météorologiques, Toulouse, France

(Manuscript received 8 February 2011, in final form 9 September 2011)

ABSTRACT

Climate change impacts on wave conditions can increase the risk of offshore and coastal hazards. The present paper investigates wave climate multidecadal trends and interannual variability in the Bay of Biscay during the past decades (1958–2001). Wave fields are computed with a wave modeling system based on the WAVEWATCH III code and forced by 40-yr European Centre for Medium-Range Weather Forecasts Re-Analysis (ERA-40) wind fields. It provides both an extended spatiotemporal domain and a refined spatial resolution over the Bay of Biscay. The validation of the wave model is based on 11 buoys, allowing for the use of computed wave fields in the analysis of mean and extreme wave height trends and variability. Wave height, period, and direction are examined for a large array of wave conditions (by seasons, high percentiles of wave heights, different periods). Several trends for recent periods are identified, notably an increase of summer significant wave height, a southerly shift of autumn extreme wave direction, and a northerly shift of spring extreme wave direction. Wave fields exhibit high interannual variability, with a normalized standard deviation of seasonal wave height greater than 15% in wintertime. The relationship with Northern Hemisphere teleconnection patterns is investigated at regional scale, especially along the coast. It highlights a strong correlation between local wave conditions and the North Atlantic Oscillation and the east Atlantic pattern indices. This relationship is further investigated at the local scale with a new method based on bivariate diagrams, allowing the identification of the type of waves (swell, storm, intermediate waves) impacted. These results are discussed in terms of comparison with previous studies and coastal risk implications.

1. Introduction

The coupled ocean–atmosphere system is of great concern for natural hazards, especially the surface gravity waves that are generated and propagate within this system. Indeed, waves are a critical parameter for risk assessment. For instance, the design of ships and offshore platforms takes into account their characteristics. Shipping also relies on wave forecast for navigation safety. Closer to the coastline, the knowledge of wave statistics is required to design coastal defenses. Waves are also one of the main phenomena responsible for shoreline evolution, where population densities in coastal regions are about 3 times higher than the global average (Small and Nicholls 2003). For instance, regarding shoreline evolution where the sediment transport is mainly cross-shore, high-energy waves usually induce shoreline erosion, whereas low-energy waves generally induce shoreline accretion and beach recovery. In summary, wave characteristic changes can lead to important modifications of the marine and coastal environment, leading to the need for human societies to adapt to these changes. Identifying past wave condition changes as well as future trends are a milestone

Corresponding author address: Elodie Charles, BRGM, 3 Avenue Claude-Guillemin, BP 36009, 45060 Orléans CEDEX 2, France.
E-mail: elodie.charles29@gmail.com

DOI: 10.1175/JCLI-D-11-00086.1

in the process of offshore and coastal risk assessment, especially in the context of climate change (Nicholls et al. 2007).

At the ocean basin scale, twenty-first-century climate simulations project a poleward shift of storm tracks (Bengtsson et al. 2006; Yin 2005) and an increase in wave height at midlatitudes (Wang et al. 2004; Wang and Swail 2006; Caires et al. 2006). At the local scale, in the North Sea, Grabemann and Weisse (2008) indicate a possible increase of 25–35 cm of the 99th percentile of significant wave heights toward the end of the twenty-first century. Thus, it has been shown that, forming a part of the ocean–atmosphere system, waves are likely to be impacted by climate change. However, quantifying the future wave climate is still a challenge regarding all the uncertainties of the system. Looking at wave characteristic evolution over the past decades is a first step in quantifying and understanding wave climate change. The analysis of wave height measurements in the North Atlantic made by Bacon and Carter (1991, 1993) indicated that there is a regular increase in the North Atlantic mean wave height of about 2.2 cm yr^{-1} from 1962 to 1986 at Seven Stones Light Vessel, and they suggested that these trends are linked to the North Atlantic Oscillation (NAO). However, their studies were based on observations over a limited spatial and temporal range. More recent studies use altimetry measurements (wave heights available since the end of 1985) (Woolf et al. 2002; Izaguirre et al. 2011) and wave hindcasts (Kushnir et al. 1997; Wang and Swail 2001, 2002; Dodet et al. 2010) to characterize past wave climates. They confirm the existence of a link between North Atlantic waves and the NAO, and show significant increases in different ranges of wave height at several northeast Atlantic locations.

The present study focuses on wave climate change in recent decades, on the French mainland Atlantic coast, bordered by the Bay of Biscay. This area is particularly exposed to energetic waves coming from the North Atlantic. In the Bay of Biscay, buoy measurements (Dupuis et al. 2006) and model outputs (Le Cozannet et al. 2011) have been analyzed and have shown opposite trends regarding the annual wave height (-1.5 cm yr^{-1} from 1980 to 2000 and 0.8 cm yr^{-1} from 1970 to 2001, respectively). It is difficult to reach a conclusion as these studies present some limitations: the Dupuis et al. (2006) analysis is based on discontinuous measurements covering a short period (20 yr) and the Le Cozannet et al. (2011) analysis is based on the wave parameters at a sole offshore point issued from the wave model of 40-yr European Centre for Medium-Range Weather Forecasts Re-Analysis (ERA40-wave) (Uppala et al. 2005). The ERA40-wave reanalysis includes uncertainties due to, among other causes, the heterogeneities of the wave data assimilation and the model quality (1.5° spatial resolution and parameterization). Thus, the long-term trend needs to be clarified, especially close to the coastline. Concerning a potential relationship with the NAO, the correlation between wave climate variability and teleconnection patterns within the Bay of Biscay is pointed out by large-scale studies covering the northeast Atlantic Ocean at a low spatial resolution. At local scale, the analysis of measured wave heights (Dupuis et al. 2006) did not bring to light a significant correlation. Le Cozannet et al. (2011) used a different approach, classifying waves issued from the ERA40-wave reanalysis at the Biscay buoy location. They established a relationship between the relative occurrence of several wave classes and the NAO index (correlation coefficients up to 0.63 for annual swell and storm classes) as well as other teleconnection patterns. Thus, it is worthwhile to assess and complete these results by spatially extending and refining the analysis.

The present work aims to characterize the spatial and temporal wave evolution during recent decades in the Bay of Biscay, in relation to climate change and teleconnection patterns.

To overcome the limitations of spatial and temporal wave data coverage, a numerical modeling approach is adopted. The model WAVEWATCH III (WW3) (Tolman 2009) is chosen to compute the waves in the Bay of Biscay during recent decades and over the whole North Atlantic Ocean to capture all waves propagating toward the French mainland Atlantic coast. Issued wave fields cover the period 1958–2001 at a spatial resolution of about 10 km. This dataset is called the Bay of Biscay wave atlas, 10-km spatial resolution hindcast (BoBWA-10kH) to differentiate it from existing datasets. It is used to investigate multidecadal trends and interannual variability of wave climate. The wave evolution for different wave height ranges and during different seasons is assessed using trends and correlation maps as well as a new method to visualize correlation on bivariate diagrams.

The paper is organized as follows. Section 2 describes the wave modeling system and its validation. The analysis of the resultant wave fields in terms of multidecadal trends and interannual variability is detailed in sections 3 and 4, respectively. Finally, conclusions are drawn in section 5.

2. Wave dynamical downscaling

a. Model setup and calibration

To provide adapted wave fields to long-term and regional wave climate analysis, a wave modeling system is set up and calibrated. The wave model and its spatial

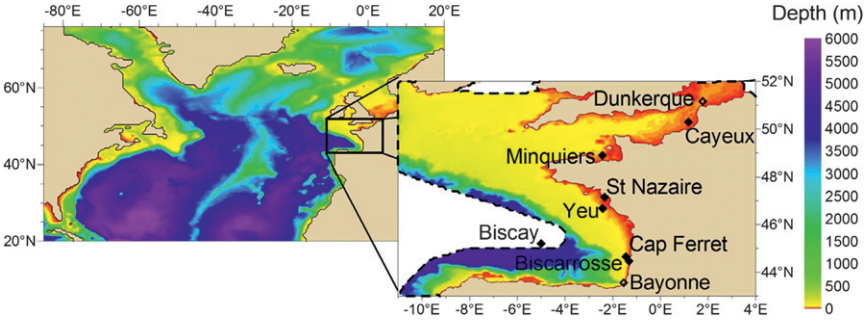

FIG. 1. Model domains with bathymetry used for the simulations with WW3 wave model. White areas (water depths > 4000 m and cells at the boundary defined as land in the first domain) are excluded from the second domain. Diamonds indicate the position of buoys used for validation. Filled diamonds indicate buoys also used for calibration. The diamond Yeu represents three different buoys, including Yeu 2 and Yeu 3, used for calibration. Minquiers and Yeu 2 are directional buoys.

coverage are described hereafter. Then, the forcing data, the calibration on the period 1998–2002, and an assessment of the impact of the wind heterogeneities induced by assimilation are detailed.

The wave hindcast is carried out with version 3.14 of WW3 (Tolman 2009). This third-generation model, developed at the National Oceanic and Atmospheric Administration (NOAA)'s National Centers for Environmental Prediction (NCEP), solves the spectral action density balance equation for wavenumber-direction spectra. The code includes wave propagation, refraction, and shoaling induced by bathymetry, wave growth, and decay due to the action of wind, whitecapping, nonlinear quadruplet wave–wave interactions, bottom friction, and depth-induced breaking. For this study, like Dodet et al. (2010), the TEST441 source terms parameterization, described in Ardhuin et al. (2010), is used. It includes improved formulations of whitecapping and wind input. This WW3 version is used in the PREVIMER forecast system (Magne et al. 2010).

Waves in the Bay of Biscay come from generation areas in the North Atlantic. They can also be generated by local wind. To consider global and local scales, waves are computed on a large domain covering the North Atlantic Ocean at a 0.5° resolution (Fig. 1). To estimate wave fields with fine spatial resolution in the area of interest, the nested approach is used with a second finer grid (0.1° resolution) covering the Bay of Biscay where water depths are less than 4000 m and coupled to the large one by a two-way nesting method. The spatial resolution of the second grid improves significantly the coastal bathymetric resolution and the land–sea limits and thus allows the use of coastal buoys (17–50-m water depths) to calibrate and validate the model. For the first grid, the 2-minute gridded elevations–bathymetry for the world (ETOPO2v2) (NGDC 2009) is used; for the second grid, the bathymetry provided by Zijderveld and Verlaan (2004) is used. The wave spectrum is meshed in 24 directions and 32 frequencies (where $f_1 = 0.0373$ Hz and $f_n = 1.1 f_{n-1}$).

The wave model is forced by the ERA-40 wind fields (ERA40-wind) (Uppala et al. 2005). They are given every 6 h at a height of 10 m, on a 1.125° × 1.125° grid. Wind is the only forcing in the wave model and Caires and Sterl (2003) showed that ERA40-wind high wind speeds were slightly underestimated. Therefore, the first step is to validate the wind data in the area of interest and, if required, to calibrate it. Measured wind speeds at a height of 3 m at the Biscay buoy are adjusted to a height of 10 m, assuming a logarithmic wind profile for neutral atmospheric conditions. The comparison of reanalyzed and measured 10-m height wind speeds at the Biscay buoy highlights that the ERA40-wind wind speeds are weaker than observed ones (bias: -0.64 m s^{-1}) and that it is necessary to correct the wind forcing.

Calibration is carried out using the period August 1998–August 2002. The wind input height is reduced to offset the underestimation of wind velocity. A sensitivity analysis is done for different values of the wind input height, varying from 2 to 10 m. The reduction of the wind input height increases the friction velocity, which is used in the WW3 code to generate and dissipate waves. The friction velocity is a function of the wind speed, the wind input height, and the water surface roughness, which varies in time and space since it depends on local wave conditions. Computed waves are compared to measured waves at eight buoys (filled diamonds in Fig. 1; deployment period and depth are given in Table 1) in terms of significant wave height, mean wave period Tm02 (determined from the zeroth and second-order moments of the spectrum), and peak wave direction. First, the simulated wave parameters are computed from the output

TABLE 1. Results of the comparison between the model and measurements: bias, RMSE, R^2, and SI are calculated for wave heights and periods; bias and RMSE are calculated for wave directions.

			Significant height				Mean period				Peak direction	
Buoy	Period	Depth (m)	Bias (cm)	RMSE (cm)	R^2	SI (%)	Bias (s)	RMSE (s)	R^2	SI (%)	Bias	RMSE
Bayonne	1989–92	20	−10	39	0.87	23	1.27	1.85	0.66	19	—	—
Biscarrosse	1980–2000	26	10	35	0.87	24	0.90	1.71	0.56	22	—	—
Cap Ferret	2001–02	54	0	28	0.92	15	0.84	1.38	0.70	16	—	—
Biscay	1998–2002	4500	−1	38	0.94	15	−0.17	0.77	0.82	10	—	—
Yeu 1	1992–98	47	−9	32	0.93	16	0.62	1.24	0.71	17	—	—
Yeu 2	1998–2000	32	−4	28	0.92	16	0.69	1.14	0.70	15	−3°	24°
Yeu 3	2000–02	32	4	30	0.94	16	0.80	1.35	0.71	17	—	—
St Nazaire	1999–2002	17	−7	25	0.77	30	1.14	1.89	0.36	33	—	—
Minquiers	1992–2000	38	−9	26	0.88	20	0.10	1.13	0.55	21	0°	36°
Cayeux	1999–2001	25	−43	58	0.85	29	−0.16	1.03	0.16	23	—	—
Dunkerque	2000–02	25	−33	45	0.76	31	−0.40	0.79	0.23	17	—	—

spectra on the same frequency band as the buoys (cutoff frequency of 0.5 Hz for the Biscay buoy and 0.625 Hz for the other buoys). Then, the squared 3-h mean (heights and periods) and 3-h mean (directions) of each dataset are calculated, resulting in a certain number of samples.

Significant wave height and mean wave period statistics [bias, root-mean square error (RMSE), squared correlation coefficient R^2, and scatter index (SI), defined as the standard deviation of the error normalized by the mean] are optimal, first at the Biscay buoy and second at the other Atlantic buoys for a wind input height value of 4.5 m (statistics for this height on the whole buoys' deployment periods are presented in section 2b). As an example, this reduction of the wind input height from 10 to 4.5 m increases the mean 10-m wind speed at the Biscay buoy by about 8%. BoBWA-10 kH wave fields are then calculated for the period 1958–2001 with the ERA40-wind wind fields given at a height of 4.5 m.

Before analyzing those wave fields in terms of trends and variability, it is relevant to check if the quality of the modeled wave fields is impacted by the increasing amount of wind measurements assimilated in the ERA40-wind reanalysis (Caires et al. 2002); more specifically, if the bias is constant during the reanalyzed period. A first investigation of the evolution of statistics (relative bias, RMSE normalized by the observed mean, SI, R^2) is done at the Biscarrosse buoy during the successive wind assimilation steps [Special Sensor Microwave Imager (SSM/I) one-dimensional variational data assimilation (1DVAR) winds since July 1987, buoy winds from the Comprehensive Ocean–Atmosphere Data Set (COADS) since June 1990, and *European Remote Sensing Satellites (ERS) 1* and *2* winds since April 1992]. The comparison of simulated waves heights with measurements from 1980 to 2000 (Fig. 2) shows no particular break in the wave statistics at these dates, even if there is a progressive reduction of statistical errors. These results suggest that the assimilation of satellite measurements in the ERA40-wind reanalysis does not result in strong heterogeneities in the modeled waves. As no measurements are available in the Bay of Biscay before 1980, it is not possible to investigate the impact of assimilation before this date. However, very few quality measurements are available and assimilated over oceans and no substantial break in the wind dataset occurs during that period. Therefore, we assume that data assimilation does not induce heterogeneities before 1980. The evolution of wave fields in the Bay of Biscay is then considered independent of ERA40-wind assimilation steps.

b. Validation of the wave modeling system

Before studying wave trends and variability over several decades and the fine temporal evolution of the wave spectrum characteristics, accurate model validation is necessary.

First, a comparison of modeled waves with a large set of measured wave data is performed. Then, the quality of the model results is compared to that of results obtained with other existing models. Finally, the emphasis is put on two buoys, to assess the performance of the model to simulate different ranges of wave height in the Bay of Biscay.

The wave modeling system is compared to 11 buoys (including two directional buoys) displaying measurements from 1980 to 2002 in both oceanic and coastal areas (Fig. 1, only the Biscay buoy is located in the coarser grid). As the present study focuses on the Bay of Biscay, the validation is done specifically against the eight Atlantic buoys. The three English Channel buoys complement the validation, allowing the estimation of the model limitations. Simulated and measured waves are compared, using the method detailed in section 2a. Bias, RMSE, squared correlation coefficient, and scatter index are displayed in Table 1.

Along the French Atlantic coast, wave height statistics are satisfactory: calculated biases are between −9 and

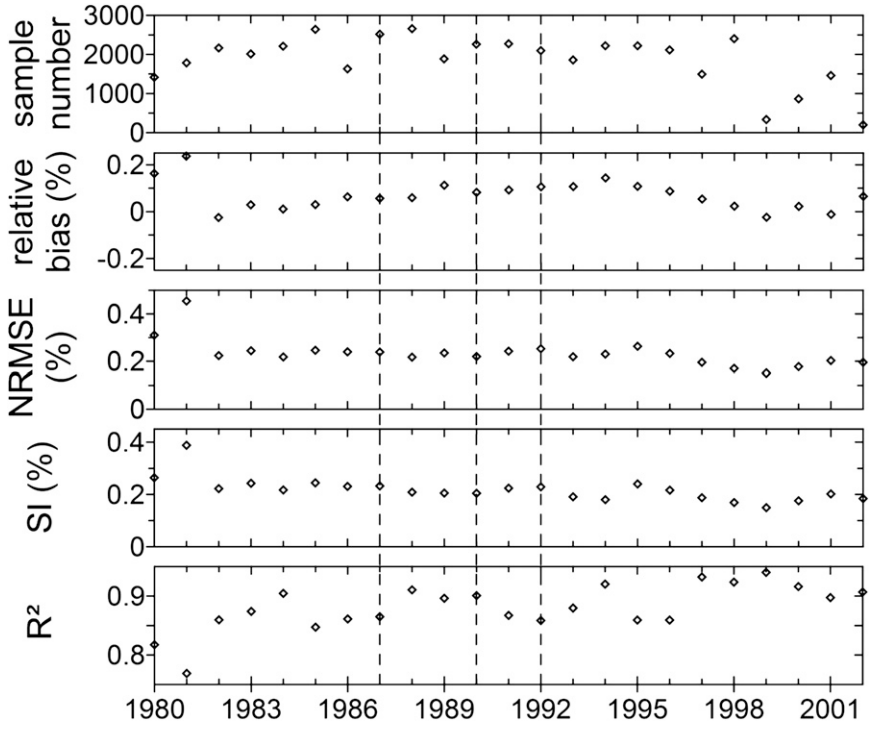

FIG. 2. Annual wave height statistics at the Biscarrosse buoy from 1980 to 2002. (top to bottom) Number of samples, relative bias, normalized RMSE (NRMSE), SI, and R^2. Vertical lines indicate the July 1987, June 1990, and April 1992 wind assimilation steps.

10 cm, RMSE fall within 25 and 39 cm, R^2 coefficients are greater than 0.77, and scatter indices are less than 30%. Modeled mean periods show good agreement with measurements at the Biscay buoy ($R^2 = 0.82$) but present a systematic positive bias of about 1 s at the other Atlantic buoys. Concerning wave directions at the Yeu 2 and the Minquiers buoys, the bias (−3° to 0°) is relatively low and RMSE (24°–36°) is satisfactory considering the directional resolution of the wave model (15°) and the spatiotemporal resolution of the wind fields (1.125° × 1.125°, every 6 h). A thorough investigation of direction time series (not detailed here) reveals a good correspondence between modeled and measured swell directions but underlines some weaknesses in the developed model to reproduce wind sea directions. This could be due to the poor wind spatiotemporal resolution and to the inability of the ERA-40 atmospheric model to reproduce coastal breeze (Žagar et al. 2006). To round off the validation against the Atlantic buoys, one can notice that the poorest correlation is obtained at the St Nazaire buoy. This can be attributed partially to the inaccurate bathymetric resolution in this coastal area. Indeed, the model water depth is 13 m, whereas the buoy is moored at 17-m depth.

In the English Channel, the quality of modeled waves at the Minquiers buoy is similar to the Atlantic ones. However, the two most eastern buoys (Dunkerque and Cayeux) show large biases and RMSE in wave height comparisons and show low correlations between modeled and measured periods. These results are mainly due to the coarse resolution that prevents the proper modeling of waves coming from the North Sea and to the fact that interactions with strong tidal currents in the English Channel are not considered here. It indicates that this model, designed for the Bay of Biscay, should not be used outside the study area.

This first part of the validation ensures good quality modeled waves in deep water in the Bay of Biscay as well as in intermediate water depths along the French mainland Atlantic coast. It guarantees that the break in the assimilated wind dataset does not induce any artificial trend. It also underlines weaknesses of the model in reproducing wind sea directions, waves in the English Channel, and wave periods along the coast (systematic positive bias of about 1 s). The lack of local measurements during 1958–79 prevents assessing the model quality during this period. The progressive reduction of error statistics at the Biscarrosse buoy (Fig. 2) is interpreted to be linked to the increasing amount of assimilated data and suggests that the wave quality is lower when going back in time.

To complete the model validation, the model performance is compared to the performance of three other existing models: the ERA40-wave reanalysis (Uppala et al. 2005), and the Dodet et al. (2010) and Digital Atlas of State Oceanic and Coastal Sea (ANEMOC) (Benoit and Lafon 2004) wave models. The ERA40-wave reanalysis is based on the Wave Model (WAM) (Komen et al. 1994) coupled to an atmospheric model. Waves are given every 6 h, at 1.5° resolution, from 1958 to 2001. Both datasets are compared to the measurements at the offshore Biscay buoy, as the spatial resolution of ERA40-wave prevents making a comparison at coastal buoys. It must be noticed that the present study dataset is optimized to fit the Biscay buoy's wave height and period. As expected, a comparison on the same time step for both models reveals that wave heights simulated by the present model (bias: 0 cm, RMSE: 39 cm, R^2: 0.93, SI: 15%) are of higher quality than wave heights issued from the ERA40-wave reanalysis (bias: −34 cm, RMSE: 55 cm, R^2: 0.93, SI: 17%). The model detailed in Dodet et al. (2010) is also based on the WW3 wave model and the Ardhuin et al. (2010) parameterization, but it is forced by wind fields issued from the NCEP–National Center for Atmospheric Research (NCAR) reanalysis (Kalnay et al. 1996) and covers the North Atlantic at a 0.5° resolution, from 1953 to 2009. The validation is based on different buoys (five buoys along Spanish and Portuguese coasts, and the ocean weather station ''Juliett'' located between Ireland and Iceland); therefore, it is not possible to make a direct comparison. A qualitative comparison can still be done at the Bilbao-Vizcaya buoy (43.63°N, 3.04°W), which is located in the Bay of Biscay. The statistical results of the comparison in 6-h windows of measured and modeled wave heights (bias: −21 cm, RMSE: 53 cm), peak periods (bias: 0.63 s, RMSE: 1.95 s), and mean directions (bias: −6°, RMSE: 20.78°) reveal that the bias and RMSE of this model are larger than our model errors for wave heights but are of the same order concerning periods and directions. More specific to French coasts, the ANEMOC database was developed with the TELEMAC-based Operational Model Addressing Wave Action Computation (TOMAWAC) wave model, with a spatial resolution near the shore of about 2–3 km. Also forced by the wind fields issued from the ERA40-wind reanalysis, waves are available from 1979 to 2001. Statistics published in Benoit and Lafon (2004) concern waves modeled in the oceanic model (variable grid size with a finer spatial resolution of 20 km near coasts) and are, a priori, better in the coastal model. The wave heights issued from the ANEMOC oceanic model from 1999 to 2000 at the Yeu 2 and Minquiers buoys exhibit a higher RMSE (37 and 33 cm, respectively) than the presently modeled waves during the same period (RMSE: 24 cm at both buoys). Thus, the present wave model is of the same or of higher quality than existing models run over a similar period and area.

Coming back to the area of interest, a thorough investigation of the quality of modeled wave heights is done by examining logarithmic histograms and quantile–quantile diagrams (correspondence between measured and simulated 1st–99th percentiles of wave heights) for two chosen buoys: Biscay and Biscarrosse (Fig. 1). Located in the middle of the Bay of Biscay (at 4500-m water depth), the Biscay buoy is exposed to swell coming from the Atlantic. The Biscarrosse buoy is located along the coast in intermediate water depth (26 m) and was deployed during the last two decades of the simulated period (1980–2001). Histograms and quantile–quantile diagrams (Fig. 3) show overall good agreement between measured and simulated wave height statistical distributions. One can notice a slight overestimation of larger wave heights at the Biscay buoy but at an order of magnitude that is acceptable for this study.

In conclusion, wave fields are well reproduced on the overall range of heights and are of similar or higher quality than other existing models in the Bay of Biscay for similar periods. Even if the model still exhibits some weakness regarding wind sea characteristics, the BoBWA-10kH dataset can be used to study long-term trends and interannual variability in the area of the Bay of Biscay.

3. Multidecadal trends

a. Method and results

Computed wave fields are available during the period 1958–2001, on the inner grid (0.1° spatial resolution), every 6 h, and at the Biscay buoy (extracted from the coarser grid), every hour. A step-by-step investigation is carried out, starting from an overview to identify periods, seasons, or wave height ranges that present significant changes in the area of interest.

Means and trends of significant wave heights, mean periods, and peak directions are computed on the whole year (January–December), winter (December–February), spring (March–May), summer (June–August), and autumn (September–November). Figure 4 represents means and normalized standard deviations (discussed in section 4) of wave heights for the period 1958–2001. Means of significant wave height vary spatially, decreasing from the open sea (about 3 m at 10°W during the whole year) to the coast (1.6 m at Biscarrosse during the whole year), and seasonally. During spring and autumn, means of significant wave height at the Biscay buoy are of the same order (2.47 and 2.55 m, respectively), whereas means

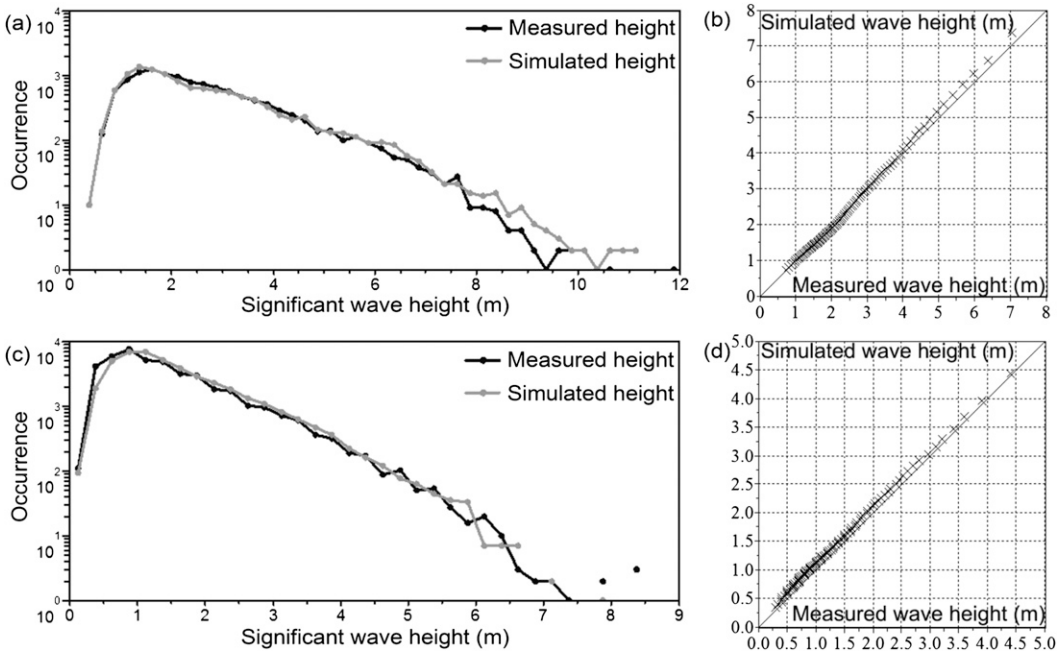

FIG. 3. (left) Logarithmic histograms and (right) quantile–quantile diagrams of significant wave height at the (top) Biscay and (bottom) Biscarrosse buoys.

of significant wave height are minimal during summer (1.56 m at the Biscay buoy) and maximal during winter (3.61 m at the Biscay buoy). The annual average is 2.54 m.

To identify multidecadal trends of significant wave heights in the Bay of Biscay, variations of annual and seasonal wave height means are first investigated at the Biscay buoy location (Fig. 5, left). The 10-yr moving average highlights three phases: 1) a decrease from 1958 to approximately 1970 (minima ranging from 1966.5 to 1972.5), 2) an increase from 1970 to approximately 1989 (maxima ranging from 1981.5 to 1995.5), and 3) a decrease from 1989 to 2001. The three identified phases, extracted from a 44-yr dataset, may indicate a 30-yr periodicity or a change of the wave climate since the 1970s. However, it must be noticed that this method does not filter the interannual variability noise. Furthermore, it can be noticed that the Fig. 2 bias and the Fig. 5 annual variations look similar. However, they are not based on the same datasets (Fig. 2 is based on highly discontinuous measurements at the Biscarrosse buoy). A thorough study of the evolution of the discontinuous modeled and measured wave heights (not shown here) indicates that the bias variations have less amplitude than the wave height interannual variations and that it does not affect the wave height trends.

The present paper's aim is to characterize present trends. Thus, the analysis focuses on the identification of trends that could have established in recent decades, that is, during periods ending in 2001. A linear regression is performed using annual and seasonal means of significant wave heights, mean periods and peak directions at the Biscay buoy during periods starting between 1958 and 1992 and all ending in 2001 (significant wave heights, Fig. 5, right). The interannual variability noise is removed by considering only trends significant at more than 95% [trends significantly different from 0 at more than 95%, according to Student's (1908) t test], which can be identified by the 95% confidence interval upper and lower bounds.

During the third phase of wave height decrease previously identified (10–20-yr periods in Fig. 5, right), it can be noticed that wave height variability is stronger since no significant trends are computed. For longer periods, statistically significant wave height trends are identified only during summer: summer wave heights increase significantly during periods starting between 1966 and 1970 and ending in 2001. The maximal significant increase, 0.54 cm yr^{-1}, is computed during the period 1970–2001 (32 yr). Calculation of trends on 20–30-yr sliding windows (not detailed here) demonstrates that the summer 1970–2001 significant trend is not isolated and lies within a homogeneous significant increase period.

Thus, the study of the summer 1970–2001 trend is extended to the whole inner grid. To assess the spatial

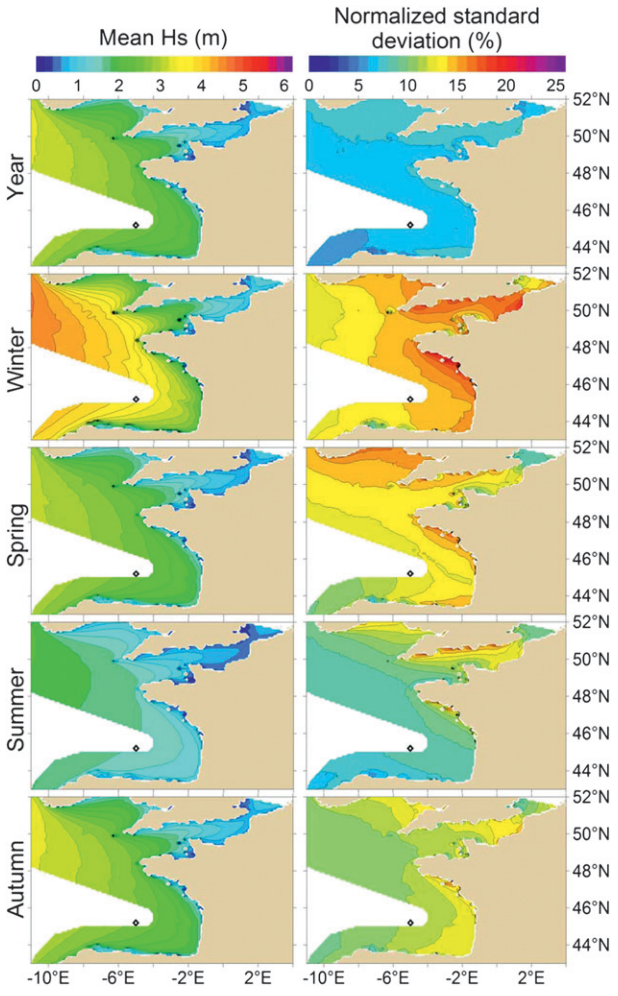

FIG. 4. (top to bottom) Annual and seasonal maps of (left) significant wave height means from 1958 to 2001 and (right) normalized standard deviation of seasonal means.

changes occurring along the French mainland Atlantic coast, a linear regression on summer wave heights from 1970 to 2001 is performed at each cell of the inner grid, for mean waves, and also for extreme waves (waves higher than the 90th and 95th percentiles' significant wave height of each cell). Figure 6 displays summer means and linear trends of the three ranges of wave height from 1970 to 2001. Trends significant at more than 95% are indicated by hatching on trend maps. It exhibits large areas of significant positive trends. The larger the considered waves (mean to the 95th percentile of significant wave heights), the larger the trends and the closer the area of significant change is to the coast. The 5% highest waves are significantly increasing over the entire French mainland Atlantic coast, by 1–2 cm yr^{-1} (32–64 cm over 32 yr).

Concerning mean wave periods at the Biscay buoy (graphs not detailed here), significant trends are identified during recent periods, starting between 1963 and 1978 and ending in 2001. Considering mean waves, summer and winter mean wave periods exhibit a significant increase of 0.009 s yr^{-1} from 1966 to 2001 and 0.018 s yr^{-1} from 1963 to 2001, respectively. The autumn mean wave periods present a significant decrease of -0.03 s yr^{-1} from 1978 to 2001. Identified trends for mean waves are significant but rarely exceed 1 s once integrated into the whole period. Regarding the wave period of extreme waves (defined as the periods of waves having wave height larger than the 90th and 95th percentiles), only spring months exhibit a significant decrease during periods starting between 1975 and 1977 (-0.047 s yr^{-1} from 1976 to 2001 for waves higher than the 90th percentile).

Wave peak directions of mean waves do not show significant trends during the whole period of 1958–2001 nor during recent decades. However, directions of spring and autumn extreme waves (defined as the directions of waves having wave heights larger than the 90th and 95th percentiles) exhibit significant trends over all of the Bay of Biscay. A significant northerly shift of spring extreme waves is computed during periods starting between 1958 and 1963 and ending in 2001 (from 1958 to 2001, 0.3° yr^{-1} at the Biscay buoy, 0.1° yr^{-1} at 2°W within the Bay of Biscay, and 0.5° yr^{-1} at 8°W for waves higher than the 90th and 95th percentiles). During autumn, a significant southerly shift of extreme waves is computed on periods starting between 1966 and 1975 and ending in 2001 (from 1974 to 2001, -0.37° yr^{-1} for waves higher than the 90th percentile and -0.47° yr^{-1} for waves higher than the 95th percentile at the Biscay buoy; -0.25° yr^{-1} at 2°W within the Bay of Biscay; and up to -0.75° yr^{-1} at 10°W for waves higher than the 95th percentile).

In conclusion, our dataset indicates a significant increase of all wave height ranges in the Bay of Biscay during the summer months from 1970 to 2001. Mean wave periods present relatively low but significant trends of decrease or increase, depending on the season, during periods starting around 1970 (between 1963 and 1978). Extreme waves' peak directions exhibit significant trends during intermediate seasons. The autumn southerly and spring northerly shifts are relatively important as they reach an absolute value of 13° at the Biscay buoy, once integrated during the trend period (1974–2001 and 1958–2001, respectively).

b. *Discussion*

The obtained results deserve to be discussed in light of previous studies. Table 2 lists recent studies of wave climatology, including the Bay of Biscay, and details each wave dataset. The main trend results issued from these studies within the Bay of Biscay are detailed in the

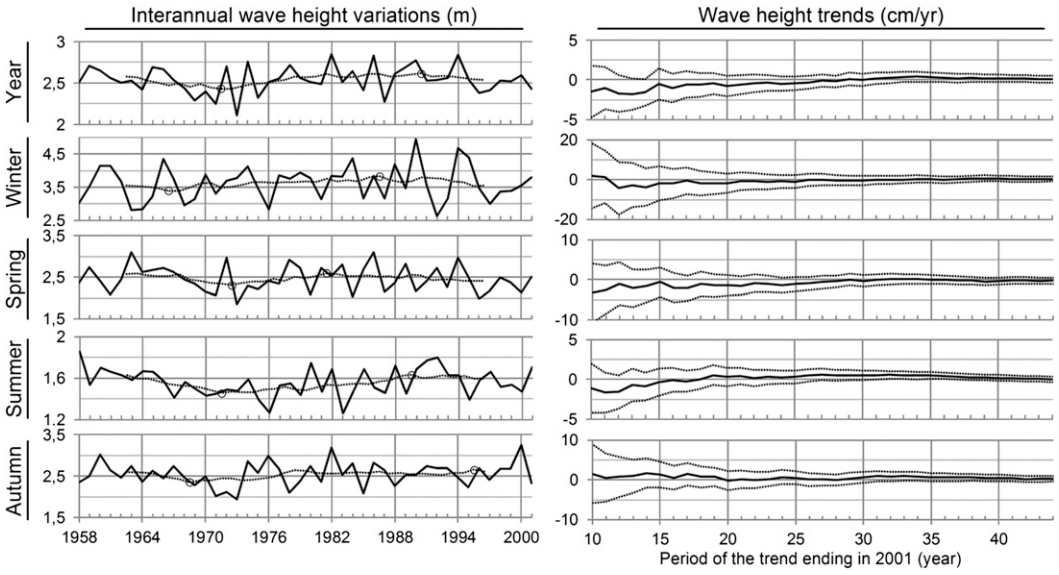

FIG. 5. (left) Evolution of (top to bottom) annual and seasonal wave heights at the Biscay buoy from 1958 to 2001 (black line) and associated 10-yr moving average (dotted line). Circles stand for the moving average minimum and maximum. (right) (top to bottom) Annual and seasonal wave height trends at the Biscay buoy on increasing periods finishing in 2001 (black line). Dotted lines are the confidence interval at 95%.

second column of Table 3. These results, in terms of multidecadal trends, are compared to the present study trends computed during the same period when possible. Then, the potential impact of the obtained trends on the sandy coast morphology is discussed.

Wang and Swail (2002) analyzed North Atlantic Ocean wave fields from 1958 to 1997, with a spatial resolution of 0.625° × 0.833° and pointed out a significant increase of the 90th and 99th percentiles of significant wave heights for latitudes north of 50°N during winter and an associate decrease south of 40°N. The area between 40° and 50°N (including the present study domain) presents no significant changes, in both winter and summer. This is consistent with the present study results: during the period 1958–97, annual and seasonal extreme wave heights exhibit no significant trends.

Dodet et al. (2010) used a higher spatial resolution (0.5°) and analyzed waves during the 1953–2009 period. The trend values for the 1953–2009 period are read on their maps (statistically significant and not significant trends are not distinguished) and are compared to the present study trends on the shorter 1958–2001 period. Their trends for the annual wave periods and directions in the Bay of Biscay are of the same order of magnitude as our trends (mainly not significant trends for the BoBWA-10kH dataset): annual peak period trends in the Bay of Biscay are of the order of 0.01 s yr^{-1} and mean wave direction trends range from 0 to 0.05° yr^{-1}. However, their trends of annual significant wave heights larger than the 90th percentile for the period 1953–2001 (0.75–1.25 cm yr^{-1} in the Bay of Biscay) are one order of magnitude larger than those found in the present study for the period 1958–2001 (not significant trends from −0.15 to 0.3 cm yr^{-1}).

The wave dataset analyzed by Woolf et al. (2002) also covers the North Atlantic Ocean, but it differs from the two latter studies as it is built from satellite measurements. It provides a large spatial coverage, with a 2° spatial resolution, during the period 1985–2000 (16 yr). The analysis of annual, seasonal, and monthly wave heights shows no significant increase trend anywhere in the North Atlantic, which is in agreement with the present study trends computed for the same period.

Concerning more local studies, Dupuis et al. (2006) analyzed the 18-yr-long time series of wave heights measured at the Biscarrosse buoy. During the period 1980–98, they pointed out the high temporal variability and did not find any increase in annual wave height but did find an insignificant decrease (−1.5 cm yr^{-1} for mean waves and −4 cm yr^{-1} for 90th percentile wave heights). An insignificant decrease was also computed for the BoBWA-10kH dataset from 1980 to 1998 with a smaller order of magnitude (−0.3 cm yr^{-1} for mean waves and −0.4 cm yr^{-1} for 90th percentile wave heights). These insignificant trends should be considered with caution as they are obtained for a relatively short period. Le Cozannet et al. (2011) analyzed the wave climate at the Biscay buoy and extended the temporal coverage of the study, using wave fields issued from the ERA40-wave reanalysis at the Biscay buoy. They applied a correction

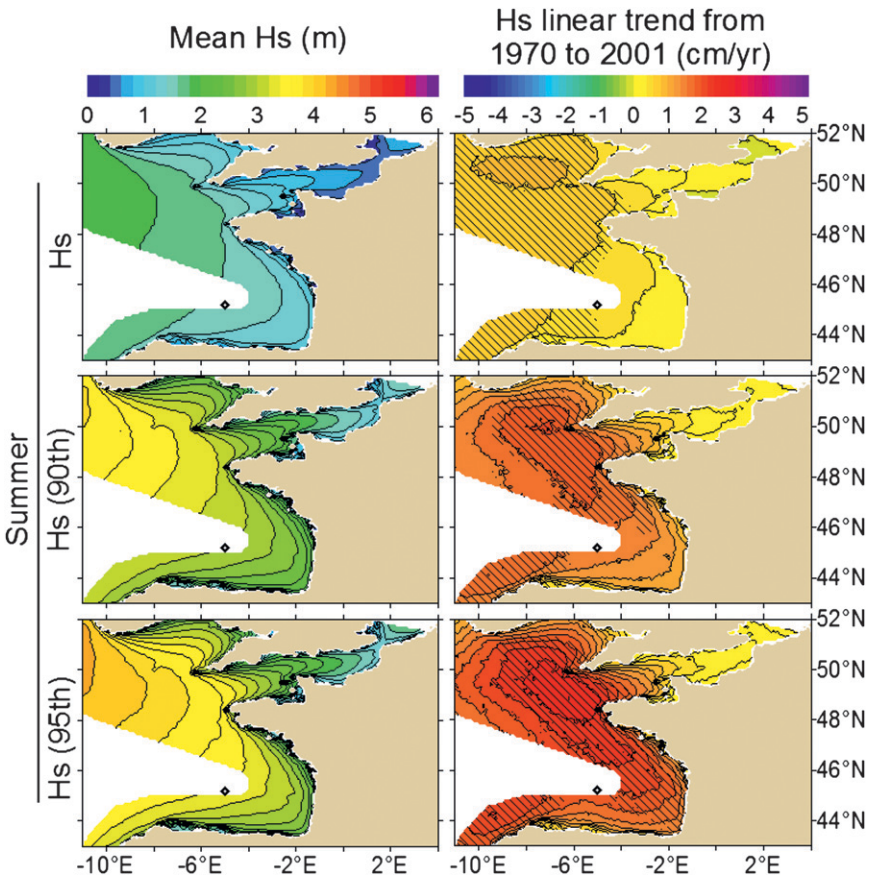

FIG. 6. Maps of (left) summer significant wave height means and (right) linear trends from 1970 to 2001 for different ranges of wave height. Hatching indicates areas with trends significant at more than 95%.

to offset the detected underestimation of wave heights by ERA40-wave at this buoy. In agreement with the present study, they obtained no significant trend during the period 1958–2001. However, they identified a significant increase in annual wave height during the period 1970–2001 (0.8 cm yr^{-1}). In the present study, annual wave heights exhibit no significant positive trends (not significant trend of 0.27 cm yr^{-1} at the Biscay buoy, which is about 3 times smaller), contrary to summer wave heights.

Thus, there are a lot of uncertainties related to models and measurements used in those studies. Among the six studies detailed here, the Wang and Swail (2002), Woolf et al. (2002), and Dupuis et al. (2006) studies did not identify significant trends in wave height, but they did

TABLE 2. Recent wave climatology studies, including the Bay of Biscay.

Reference	Area	Period	Source of data
Wang and Swail (2002)	North Atlantic	1958–97	Oceanweather's 3G wave model (0.625° lat × 0.833° lon) forced by 6 h ERA-40 reanalysis wind with kinematic analysis
Woolf et al. (2002)	North Atlantic	1985–2000	Satellite-derived wave climatology (2° lat–lon)
Dodet et al. (2010)	Northeast Atlantic	1953–2009	WW3/TEST441 wave model (0.5° lat–lon) forced by 6-h NCEP–NCAR reanalysis wind (1.905° lat × 1.875° lon)
Dupuis et al. (2006)	Biscarrosse buoy (44.46°N, 1.32°W)	1980–98	Buoy measurements
Le Cozannet et al. (2011)	Biscay buoy (45°N, 5°W)	1958–2002	ERA-40 wave reanalysis (0.5° lat–lon) corrected using buoy measurements
This study	Bay of Biscay	1958–2001	WW3/TEST441 wave model (0.1° lat–lon) forced by amplified 6-h ERA-40 wind (1.125° lat–lon)

TABLE 3. Wave parameter trends and correlation with teleconnection patterns within the Bay of Biscay issued from studies detailed in Table 2. For each result, the following complementary information is given: [trend period or teleconnection pattern] wave parameter (associated period). The wave parameters are Hs (significant wave height), Hs10 (10% smallest wave heights), Hs90 and Hs99 (90% and 99% highest wave heights, respectively), Tp (peak period), and Dm (mean wave direction). The associated periods are An (annual), Wi (winter), Sp (spring), Su (summer), and Au (autumn).

Reference	Trends	Correlation with NAO and EA
Wang and Swail (2002)	[1958–97] Hs90 (Wi/Su/Au); Hs99 (An/Wi/Au): not significant	Not investigated
Woolf et al. (2002)	[1985–2000] Hs (An/Wi/Sp/Su/Au): not significant	[NAO] Hs (Wi): $R = 0.4$–0.5
Dupuis et al. (2006)	[1980–98] Hs10 (An): -0.7 cm yr^{-1}; Hs (An): -1.5 cm yr^{-1}; Hs90 (An): -4 cm yr^{-1}	[NAO] Hs (An): $R = 0.066$; Tm (An): $R = 0.38$
Dodet et al. (2010)	[1953–2009] Hs90 (An): 0.75–1.25 cm yr^{-1}; Tp (An): 0.01 s yr^{-1}; Dm (An): 0 to -0.03 yr^{-1}	[Wi-NAO] Hs90 (An): $R = 0.2$–0.4; Tp (Wi): $R = 0.55$–0.65; Dm (Wi): $R = 0.15$–0.3
Le Cozannet et al. (2011)	[1958–2001] Hs (An): not significant; [1970–2001] Hs (An): significant and 0.8 cm yr^{-1}	[NAO] swell class (Wi): $R = 0.4$; wind sea class (An): $R = -0.31$; intermediate class (An/Wi): $R = -0.39/-0.54$; [EA] storm class (Wi): $R = 0.52$; wind sea + intermediate classes (Wi): $R = 0.54$

not test periods different from the maximal period covered by their datasets. Computed for the same periods, the present study trends are also insignificant. The other three studies tend to show an increase in wave height in the Bay of Biscay. This increase concerns annual wave heights for Dodet et al. (2010) and Le Cozannet et al. (2011), whereas in the present study this increase in mean and extreme wave height is noticeable only during summer and not during the rest of the year.

The increase in the summer mean and extreme wave height identified in the present study is relatively important and can potentially impact sandy coasts. Indeed, summer is a period of accretion for most sandy coasts, and a strengthening of the wave climate during the recovery period of beaches could limit this phase of accretion. Moreover, Castelle et al. (2010) underlined that the beach system is quite sensitive to changes in low-energy wave height. Indeed, they show that above a certain wave height threshold, close to 1 m, a change in the morphological response of the beach is noticeable. The value of this threshold is relatively close to the summer wave height means computed by the present model at depths of 20 m along the Aquitanian coast. The present estimated increase could indicate more waves with heights higher than this threshold, which could then induce a change in the beach morphology.

Regarding other wave parameters, the identified trends in autumn and spring extreme wave directions can impact the longshore sediment transport along the coast. Depending on the spatial distribution of wave directions along the coast, the longshore sediment transport could vary and induce more erosion or accretion in certain areas and also modify the local beach dynamics (bar changes). A better representation of wave directions nearer to the coast and considering bathymetric refraction is required to assess this impact.

4. Interannual variability

a. Teleconnection patterns

Waves are directly generated by winds in different areas of the globe; therefore, global atmospheric circulation plays an active role in regional wave climates. The global atmospheric circulation description can be simplified into different preferred patterns, useful to understand and even to predict changes in temperature, precipitation rates, and wind and wave conditions (Hurrell et al. 2003; Woolf et al. 2002; Seierstad et al. 2007; Cassou 2008). In the area of interest, Dupuis et al. (2006) and Le Cozannet et al. (2011) compared wave condition variations to selected Northern Hemisphere teleconnection pattern indices defined by Barnston and Livezey (1987) (indices can be downloaded from the Climate Prediction Center website at http://www.cpc.ncep.noaa.gov/data/teledoc/telecontents.shtml). This approach is used for the present results as a preliminary investigation of the potential relationships between the local wave climate and large-scale patterns. Therefore, among the 10 leading teleconnection patterns investigated, only the results with the predominant patterns over the study area—the NAO and the East Atlantic (EA) pattern—are detailed here.

First, the investigation of wave climate variability and correlation with teleconnection patterns is done on the whole Bay of Biscay (section 4b). Contributions of predominant teleconnection patterns are assessed by correlation maps between wave characteristics and teleconnection pattern indices. Second, a more detailed

TABLE 4. Significant correlation coefficients between seasonal teleconnection pattern indices and seasonal significant wave heights, mean periods, and peak directions. Mean correlation coefficients are computed in the area limited by 5°W and 48°N. Correlation coefficients are also given at the Biscay (Bi) and the Biscarrosse (Br) buoys locations. Only significant coefficients are shown (probability that the relationship is fortuitously higher than 95% by *t* test). Coefficients with an absolute value larger than 0.5 are in boldface.

		Hs			Tm			Dp		
		Mean	Bi	Br	Mean	Bi	Br	Mean	Bi	Br
NAO	Winter	0.38	0.33	0.32	**0.51**	**0.55**	0.35	0.32	—	0.36
	Spring	—	—	—	0.45	0.45	0.44	—	—	—
	Summer	−0.43	−0.43	−0.47	—	—	—	0.37	—	0.45
	Autumn	—	—	—	0.44	0.45	0.41	0.35	0.34	0.47
EA	Winter	**0.57**	**0.58**	**0.60**	**0.50**	**0.51**	**0.55**	**−0.55**	**−0.72**	**−0.72**
	Spring	0.32	0.32	0.33	—	—	—	—	—	—
	Summer	**0.52**	**0.52**	**0.53**	—	0.34	—	—	—	—
	Autumn	0.44	0.42	0.44	0.37	0.40	0.30	—	—	−0.30

analysis based on bivariate diagrams at one buoy location (section 4c) is done to determine if the predominant teleconnection patterns contribute to preferred parts of the wave spectrum.

Before going further, it should be noted that local wave characteristics and teleconnection pattern indices are of different nature and cover different spatial scales. Waves are directly generated by surface winds, which are linked to the global atmospheric circulation but also propagate to areas with different wind conditions, and are impacted by local variables, such as bathymetry. Teleconnection pattern indices describe the global atmospheric circulation over large parts of the globe. This implies that correlation coefficients between waves and indices will be smaller than typical correlation coefficients between variables of similar nature. Coefficients larger than 0.5 thus indicate a relatively strong correlation between a given type of wave and the teleconnection pattern (Bacon and Carter 1993).

b. Spatial correlation

Interannual variability is examined over the entire inner grid using maps of wave height normalized standard deviation. Then, the correlation between wave parameters and teleconnection patterns is investigated using correlation maps. Maps for seasons with the most significant correlation coefficients between wave height, period, and direction, and teleconnection patterns are analyzed in more detail. Correlation coefficients for all seasons are synthetized in Table 4.

First, as an overview of the order of magnitude and of the spatial distribution of the wave height interannual variability, maps of normalized standard deviation, computed from the annual and seasonal significant wave height means, are plotted during the period 1958–2001 (second column in Fig. 4). The interannual variability of annual significant wave heights is spatially homogeneous, with normalized standard deviations of about 6% in the Bay of Biscay. On the contrary, the interannual variability of seasonal significant wave heights is larger and presents spatial heterogeneities. The normalized standard deviation is larger in winter, with maximal values observed along the coast (larger than 15%), and smaller in summer, with decreasing values from north to south (from 5% to 10% in the Bay of Biscay).

To assess the amount of the variability related to teleconnection patterns, the variations are compared to the teleconnection pattern index variations. Seasonal anomalies of significant wave height, mean period, and peak direction are computed for each point of the inner grid. The seasonal variations of these anomalies are then compared to the seasonal variations of the teleconnection pattern indices, resulting in maps of correlation coefficients. Areas presenting significant correlation coefficients (at more than 95% by a Student's *t* test) are indicated by hatching. In the Bay of Biscay, among the examined teleconnection patterns, the NAO and EA are predominant, as expected as they both present maximal variance over the North Atlantic Ocean. This agrees with Izaguirre et al.'s (2011) results: they investigated the influence of 10 climate patterns on extreme wave height issued from satellite data at a global scale and identified a significant contribution of NAO and EA indices in the northeast Atlantic Ocean, between 40° and 60°N. Maps of correlation coefficients between wave characteristics and NAO and EA indices are presented in Fig. 7 for the two seasons (winter and summer for NAO, and winter and autumn for EA) that show the most significant correlations.

Concerning the NAO, direct correlations with significant wave height, mean period, and peak direction are observed in winter (Fig. 7), whereas in summer significant wave heights present an inverse correlation with NAO indices. During winter, the positive phase of the NAO [corresponding to a stronger subtropical high pressure over the Azores and a deeper Icelandic low

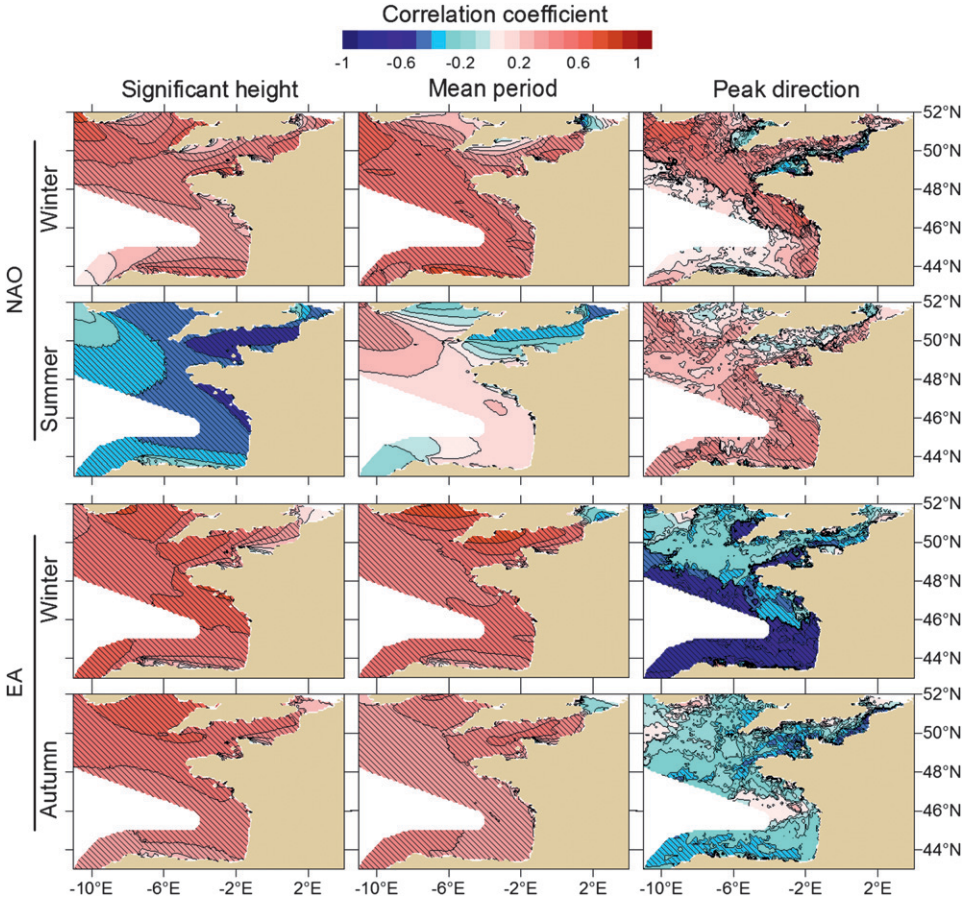

FIG. 7. Maps of correlations between (top to bottom) seasonal NAO and EA teleconnection pattern indices and (left to right) seasonal significant wave heights, mean periods, and peak directions from 1958 to 2001 for selected seasons. Hatching indicates areas with correlation coefficient significant at more than 95% (Student's *t* test).

(NAO+)] is associated with an increase in significant wave height and mean period, and a northerly shift in wave peak direction. During summer, the NAO+ is associated with a decrease in significant wave height ($R = -0.43$ averaged in the Bay of Biscay) and a northerly shift in wave peak direction ($R = 0.37$ averaged in the Bay of Biscay). The analysis of spatial variations shows a stronger correlation with the winter wave height southwestward of Ireland. More locally, in the Bay of Biscay, the correlation increases from north ($R = 0.3$) to south ($R = 0.6$). The spatial distribution is reversed during summer: the correlation is negative, stronger to the north of the Bay of Biscay and weaker southwestward of Ireland.

Concerning the EA, moderate to strong correlations are observed for each season between EA indices and significant wave heights. The positive phase of the EA [corresponding to a deeper low in the North Atlantic at approximately 50°–55°N and a higher subtropical high (EA+)] is associated with an increase in significant wave height and mean period. During winter, a strong correlation is noticeable for all wave parameters in the Bay of Biscay (mean correlations higher than 0.5). The EA+ is then associated with a southerly shift in wave peak direction. The correlation coefficients are globally stronger in the area between Ireland and England. In the Bay of Biscay, correlation coefficients between EA indices and significant wave height anomalies increase from south ($R = 0.2$ during winter) to north ($R = 0.7$ during winter).

To synthetize the results, Table 4 lists the significant correlation coefficients (95% by a Student's *t* test) between wave parameters and the NAO and EA indices during each season. Spatially averaged correlation coefficients are computed in the Bay of Biscay (area eastward of −5°E and southward of 48°N), and local correlation coefficients are computed at the Biscay and Biscarrosse buoy locations to estimate the extent of the correlation from offshore to the coast. Globally, the spatial distribution is homogeneous from west to east: correlation

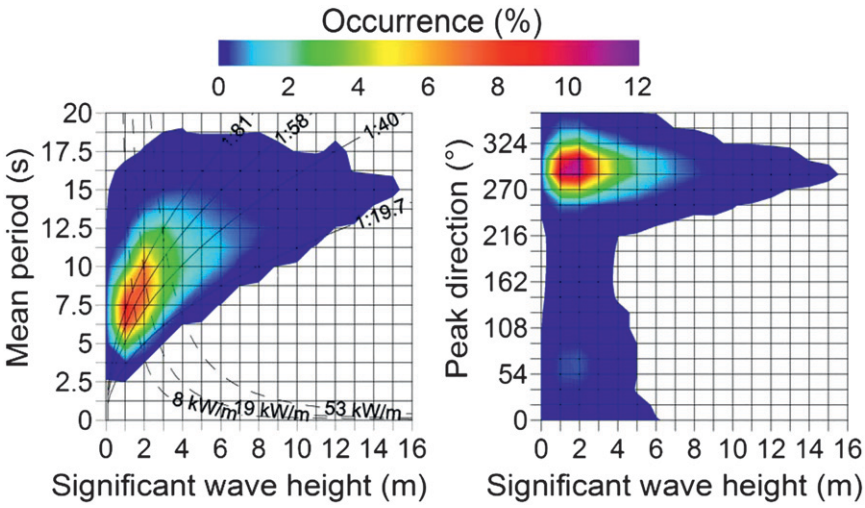

FIG. 8. Bivariate diagrams of significant wave height with (left) mean period and (right) peak direction, plotted from the wave conditions modeled from 1958 to 2001 at the Biscay buoy. Color shading indicates the occurrence of waves in each cell (%). Solid lines indicate the wave steepness isolines, and dashed lines show wave energy flux isolines.

maps (Fig. 7) and correlation coefficients extracted at buoys (Table 4) confirm that correlation coefficients obtained offshore and along the coast are quite similar for points located at the same latitude. Correlation coefficients vary from north to south, with a gradient depending on the teleconnection pattern, the season, and the wave parameter. However, the sign of the correlation remains globally constant inside the area delimited by the inner grid.

To summarize, the results in the Bay of Biscay highlight strong correlations between teleconnection patterns (NAO and EA indices) and wave characteristics (significant wave height, mean period, and peak direction) during almost all seasons. The spatial distribution is relatively homogeneous in the Bay of Biscay and particularly along the east–west axis.

c. *Local correlation*

Teleconnection patterns and seasons presenting high correlations with wave parameters in the Bay of Biscay are identified. To determine which types of waves are correlated with teleconnection patterns, a thorough examination is carried out at the Biscay buoy location.

The variability of wave characteristics is investigated using bivariate diagrams of wave densities (distribution of wave heights against periods and of wave heights against directions), for different seasons. To calculate wave densities, bivariate diagrams are divided into cells of 1 m, 1.25 s, and 18° for significant wave heights, mean periods, and peak directions, respectively. Bivariate diagrams illustrating the annual wave characteristics during the whole period (1958–2001) at the Biscay buoy location are plotted in Fig. 8. During the whole period, the most frequent waves have a significant wave height of 1 m, a mean period of 6.25–7.5 s, and a peak direction of 288° (west-northwest).

Steepness and energy flux of waves at the Biscay buoy are detailed on the bivariate diagram of wave height against wave period. Using the linear theory and the assumption of deep water, the wave energy flux is defined as $F = \rho T_m g^2 H_s^2/64\pi$, where ρ is the water density, T_m is the mean wave period, g is the acceleration of gravity, and H_s is the significant wave height. Isolines of each quartile of the wave energy flux at the Biscay buoy are plotted. Using the linear theory, wave steepness in deep water is related to the mean period by the following formula: $\epsilon = 2\pi H_s/gT_m^2$. Wave steepness is an indicator of the wave age: usually, young waves generated locally present a large steepness, whereas older waves propagating from distant areas present a smaller steepness. Isolines of each quartile of wave steepness at the Biscay buoy are plotted. A fourth isoline of steepness $\epsilon = 1/19.7$ represents the constant steepness obtained by Pierson and Moskowitz (1964) in the case of idealized fully developed wind seas.

Then, seasonal wave density anomalies are determined by subtracting in each cell the seasonal densities from the period 1958–2001 from the seasonal densities of each year, resulting in seasonal density anomalies. To go further in the analysis of the link with teleconnection patterns, variations and amplitudes of the annual density anomalies are considered. First, the variations are compared to the teleconnection pattern indices of the corresponding season, resulting in a bivariate diagram of correlation. Then, the average of

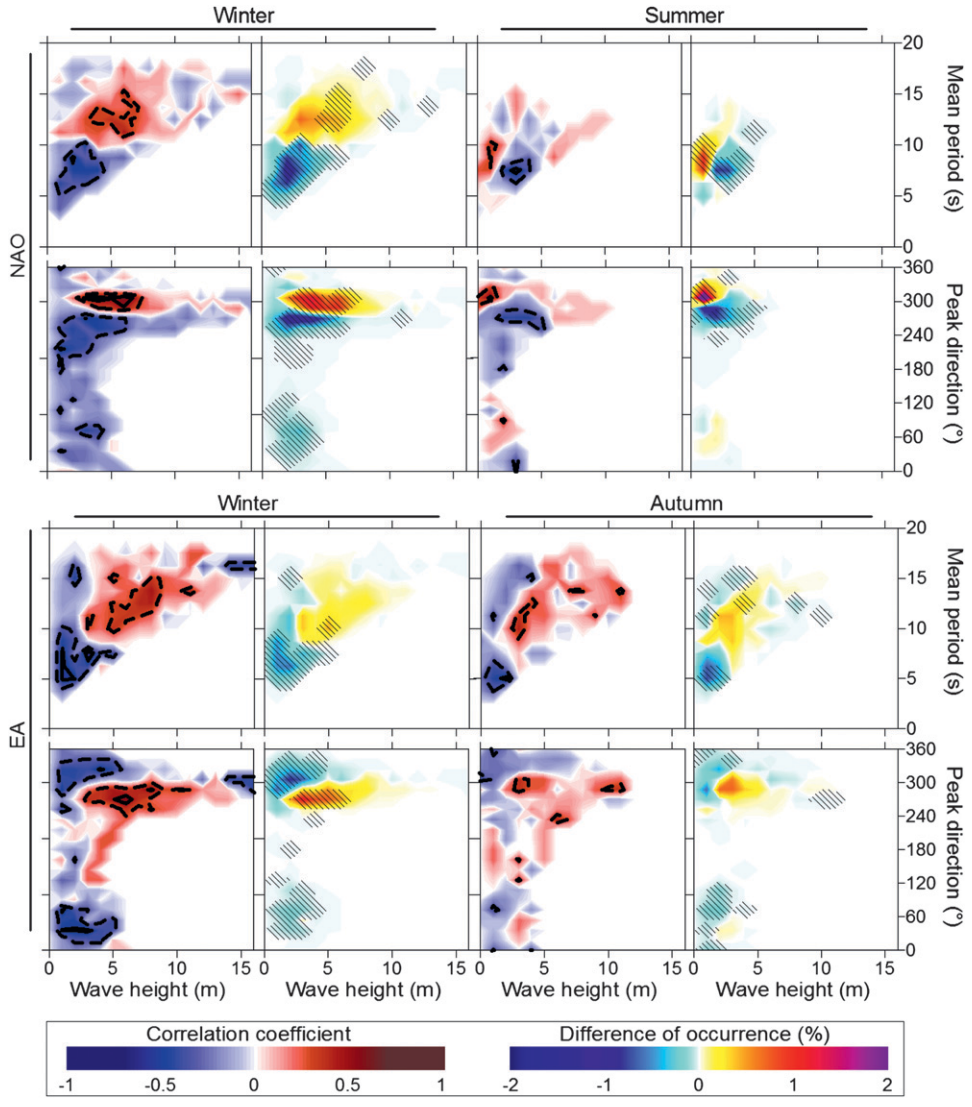

FIG. 9. Correlation bivariate diagrams for the (top) NAO and (bottom) EA and associated bivariate diagrams of density anomalies during the positive phase years at the Biscay buoy. Hatching indicates cells with a mean density significantly different from 0 (probability higher than 90% by *t* test).

the density anomalies of every year with a positive phase are computed, resulting in a bivariate diagram of density anomalies during the positive phase of each teleconnection pattern. The amplitude during negative phases is quite similar to the amplitude during positive phases (presenting an opposite sign) and is thus not shown here. Significant amplitudes (means statistically different from 0 at a probability higher than 90% by a Student's *t* test) are highlighted by hatching on bivariate diagrams. NAO and EA teleconnection patterns are examined thoroughly (Fig. 9) during seasons selected in the analysis of correlation maps.

The study of bivariate diagrams (Fig. 9) related to the NAO highlights different correlation patterns during winter and summer. During winter, an increase of the NAO index is linked to an increasing occurrence of large waves and to a decreasing occurrence of waves with periods shorter than 10 s and heights smaller than 5 m. During summer, the patterns of correlation are different: the NAO index increase is related to an increase of swell and a decrease of intermediate wave (young waves, with short periods relative to wave height) occurrence. Concerning wave directions, winter and summer bivariate diagrams show the same northerly shift that is strongly related to an increase of the NAO index.

Bivariate diagrams related to the variations of EA indices during winter and autumn (Fig. 9) exhibit similar patterns of correlations and anomalies. Large wave

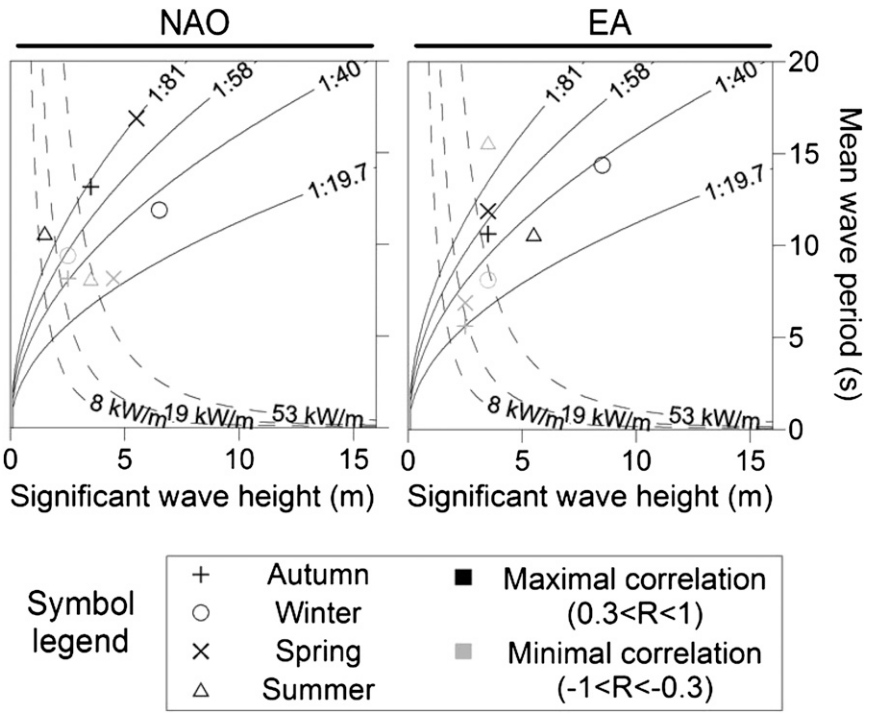

FIG. 10. Bivariate diagrams summarizing the locations of minimal value (maximal negative value, gray symbols) and maximal value (maximal positive value, black symbols) of correlation coefficients between the NAO, EA, and wave density anomalies during each season. Solid lines indicate the wave steepness isolines, and dashed lines show wave energy flux isolines.

(including intermediate waves, swell, and storms) occurrence increases with the EA index, whereas the occurrence of waves smaller than 3 m decreases. A southerly shift in the wave direction is noticeable during winter and autumn.

Concerning the correlation of the NAO and EA with wave density anomalies during other seasons, a synthesis of the results of bivariate diagrams of significant wave height against the mean period is given in Fig. 10. The positions of the minimal (maximal negative value, in gray) and maximal (maximal positive value, in black) correlation coefficients on bivariate diagrams are plotted for the NAO and EA for each season (indicated by symbols). Locations of extrema of correlations on the bivariate diagrams indicate a different action of teleconnection patterns, depending on the season. To better understand the action of teleconnection patterns, isolines of wave steepness and wave energy flux (previously described for Fig. 8) are plotted.

For the NAO and EA, positions of maximal and minimal correlation coefficients on bivariate diagrams of wave height against the period clearly show a different level of wave energy flux during winter and a different level of steepness during summer. In winter, the wave steepness of minimal and maximal correlation coefficients is quite similar for the NAO and EA, whereas isolines of wave energy flux clearly separate the maxima and minima of each teleconnection pattern. The position of the winter minimal correlation coefficient indicates waves having an energy flux between 19 and 53 kW m^{-1}, and the position of the maximal correlation coefficient indicates very energetic waves, with an energy flux higher than 200 kW m^{-1}. Then, an increase of the NAO and EA can be linked to an increase of storminess in generation areas, resulting in more energetic waves at the Biscay buoy. During summer, wave energy flux isolines are quite similar for the maxima and minima of each teleconnection pattern, whereas wave steepness isolines ($\epsilon = 1/58$) isolate the minima from the maxima of each teleconnection pattern. This could mean that during summer, teleconnection pattern index variations do not modify much wind intensity but do modify the distance of the wave generation areas from the Bay of Biscay. During intermediate seasons, NAO and EA influence both steepness and energy flux, which would suggest an influence of the teleconnection patterns on the wind speed and on the distance of wave generation areas from the Bay of Biscay during autumn and spring.

d. Results analysis

Specific changes in significant wave height, peak period, and peak direction appear to be linked to NAO and

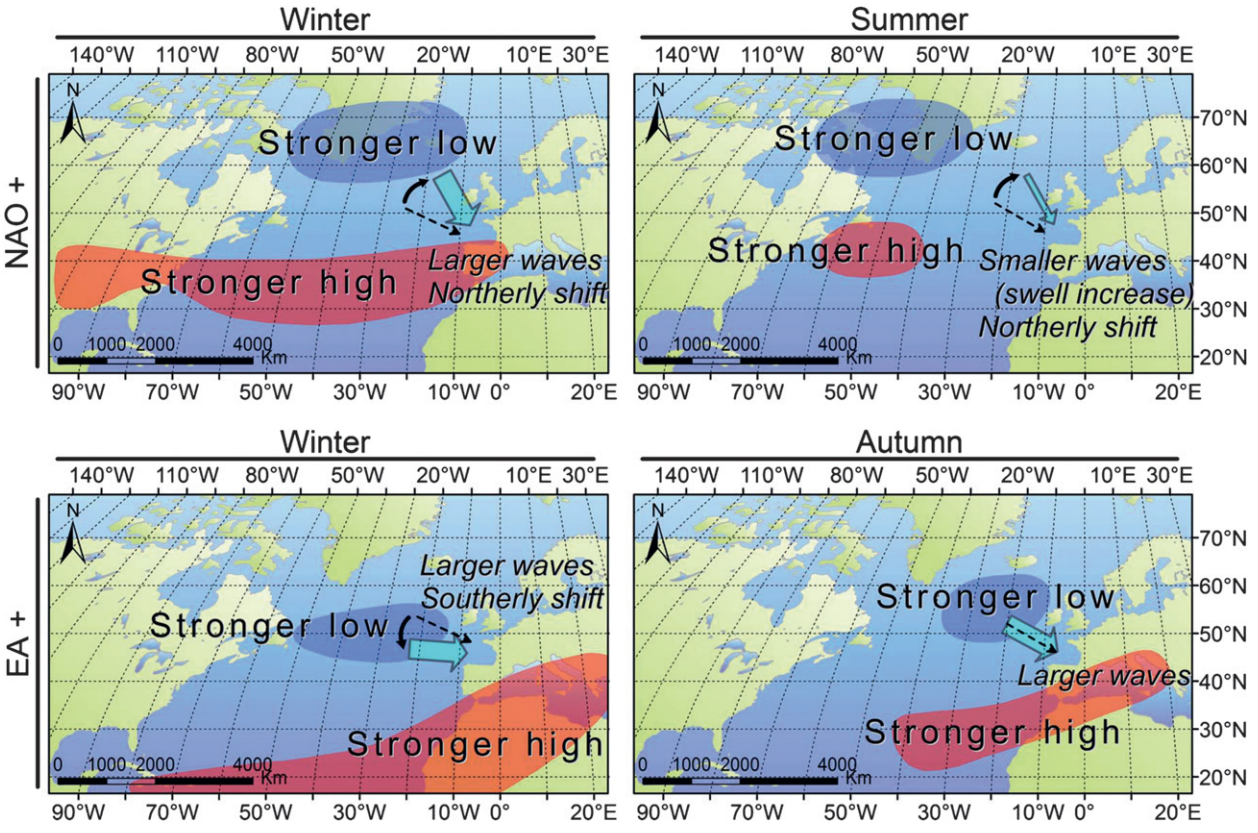

FIG. 11. Maps of seasonal standardized 500-mb geopotential height anomalies for the positive phase of the specified teleconnection pattern and season (adapted from http://www.cpc.ncep.noaa.gov/data/teledoc/nao_map.shtml and http://www.cpc.ncep.noaa.gov/data/teledoc/ea_map.shtml) and associated changes in wave conditions in the Bay of Biscay according to this study. Dotted arrows indicate the mean wave direction during the specified season, and blue arrows indicate the direction changes (not at scale) and their thickness indicates the wave height evolution.

EA patterns. To study this link, it is necessary to better understand the link with global atmospheric circulation. Figure 11 gives an overview of the seasonal mean standardized 500-mb geopotential height anomalies during the positive phase of the NAO and EA during different seasons. Associated changes in wave conditions in the Bay of Biscay are indicated by arrows. During the negative phase of EA and NAO, the 500-mb geopotential height anomalies are reversed, resulting in a weaker low and high. These anomalies are mainly located in the North Atlantic Ocean, in the primary wave generation area spreading from the east coast of North America toward the Norwegian Sea (Alves 2006).

The predominance of the NAO in the established relationships was brought to light in many studies (Bacon and Carter 1993; Woolf et al. 2002; Dodet et al. 2010; Le Cozannet et al. 2011). This strong correlation can be explained by the stronger-than-usual and northerly shifted (weaker and southerly shifted) winds occurring over the North Atlantic Ocean during the NAO+ (NAO−) phase (Fig. 11). Those winds impact waves that propagate to the French mainland coast. In the present study focusing on the Bay of Biscay, during winter waves present larger (smaller) significant wave heights and a northerly (southerly) shift during the NAO+ (NAO−) phase. However, during summer, this correlation is reversed with smaller (larger) significant wave heights occurring more frequently during the NAO+ (NAO−) phase. One plausible explanation could be the northwestward shift of the north–south dipole of height anomalies occurring during summer (Fig. 11). Wave generation areas usually located in the north-central part of the North Atlantic during winter would move toward Canada and Greenland during summer. Long-period swell propagating from this more distant area would occur more frequently and intermediate and storm waves generated more locally would occur less frequently during summer. Another explanation could be a different sensitivity of the summer and winter wave characteristics to the negative and positive phases of the NAO. To go further, it is necessary to study the sensitivity of winter and summer wind and wave characteristics to the NAO+ and NAO−.

A link between the EA and winter wave climate was previously established and commented on by Seierstad et al. (2007) and Le Cozannet et al. (2011). Like the NAO, the EA pattern consists of a north–south dipole of anomalies, but its centers are located southward (Fig. 11). Its positive phase (EA+) is associated with an anomalous low reaching the Bay of Biscay on its northeastern side (Seierstad et al. 2007). Strong winds generate waves near the French mainland coast, leading to an increase of energetic waves during that phase. The southerly shift in wave direction is also directly related to the increased storminess in this north-central part of the North Atlantic Ocean.

To conclude, the present study underlines strong correlations between wave interannual variability and NAO and EA Northern Hemisphere teleconnection patterns. In particular, NAO and EA teleconnection pattern indices are correlated to an increase in wave height and period during winter and to a northerly and southerly shift in wave direction, respectively. During summer, the reversal of the correlation between the NAO index and significant wave heights would require further investigation. The NAO and EA thus play a role in wave climate variability.

e. Discussion

As detailed in section 4d, previous studies highlighted the high interannual variability of wave fields in the North Atlantic and in the Bay of Biscay, and correlated it to several teleconnection pattern indices. The following discussion is based on the most recent studies (Table 2), including the Bay of Biscay. The main results issued from these studies within the Bay of Biscay are summarized in the third column of the Table 3.

Le Cozannet et al. (2011) used a different approach from the present study. They classified waves at the Biscay buoy location (issued from the ERA40-wave reanalysis) into 12 wave classes using the *K*-means algorithm, each class representative of a sea state at the Biscay buoy. They compared annual and seasonal wave class occurrences to teleconnection pattern indices. As in the present study, they found a strong and direct correlation between NAO indices and high-energy swell classes during winter ($R = 0.40$), and an inverse correlation with wind sea ($R = -0.31$) and intermediate wave classes ($R = -0.39$) during the whole year, appearing to be greater during winter ($R = -0.54$). During winter, they also found strong correlations between the EA and storm classes ($R = 0.52$) and wind sea grouped with intermediate wave classes ($R = -0.54$). These patterns are also highlighted in the present study: during winter, the results indicate a strong and inverse correlation between EA indices and waves smaller than 3 m (minimal correlation coefficient value on EA winter bivariate diagram in Fig. 9 is −0.59), and a strong and direct correlation with energetic swells, intermediate waves, and storms (maximal correlation coefficient value on EA winter bivariate diagram is 0.47).

Still in the area of interest, Dupuis et al. (2006) computed correlation coefficients between annual NAO indices and annual wave parameters at the Biscarrosse buoy (1980–98), obtaining no significant correlation with mean wave heights ($R = 0.066$) and a moderate correlation with mean wave periods ($R = 0.38$). They emphasized that the period of comparison (1980–98) was certainly too short to encounter a sufficiently large range in the NAO index. Finally, Dodet et al. (2010) globally found a strong correlation between the NAO index and wave heights southwest of Ireland. In the Bay of Biscay, they found weak to strong correlations between winter NAO indices and the annual 90th percentile of wave heights ($R = 0.3$ at the Biscay buoy), the winter means of mean wave direction ($R = 0.15$ at the Biscay buoy), and peak period ($R = 0.6$ at the Biscay buoy). Correlation coefficients of the same magnitude order were obtained in the present study; however, the investigation of each season separately highlighted some differences, particularly for directions for which correlation coefficients higher than 0.5 were computed.

These studies show that interannual variability of wave characteristics in the Bay of Biscay are linked to the NAO and EA, and that this link is more or less pronounced for certain seasons, wave height percentiles, classes, or ranges of wave heights, periods, and directions. These different behaviors show the relevance of clustering waves (according to their height, period, and direction characteristics and also according to seasons) to better assess the impact of the global atmospheric circulation, described by teleconnection pattern indices.

The present study highlights the link between waves and teleconnection patterns, with phases exhibiting more energetic waves than usual. Considering coastal risk implications, a relation between teleconnection patterns and coastal evolution can also be found. For instance, Ranasinghe et al. (2004) showed that the observed severe erosion of embayed beaches in New South Wales, Victoria, Australia, was not associated with severe storm events nor with any long-term recession tren, but with the alternation of El Niño–La Niña phases. They identified the physical processes induced by the Southern Oscillation index cycle that lead to a rotation of embayed beaches. In the area of this study, Parisot et al. (2010) identified a link between NAO indices and sand volume variations of the Truc Vert beach (Aquitaine coast, France), which could confirm the role of teleconnection patterns in the French mainland coastal evolution. In the

present study, NAO indices are indeed strongly related to erosive events, such as energetic swells and storms. Terray et al. (2004) suggest that the winters of the late twenty-first century will be characterized by an increase (decrease) of the NAO+ (NAO−) climate regime occurrence. Thus, the wave climate in the Bay of Biscay could be more energetic and induce more erosive events along the French mainland Atlantic coast.

5. Conclusions

In this paper, the long-term trends and the interannual variability of wave climate in the Bay of Biscay during recent decades were investigated. A wave modeling system, based on the WAVEWATCH III numerical model, was setup to provide wave fields at a high spatial resolution (10 km) and temporal coverage (1958–2001) along the French mainland Atlantic coast. Its accurate validation allowed the thorough analysis of wave fields in terms of mean wave heights as well as extreme wave heights (90th and 95th percentiles of wave heights).

The thorough examination of wave parameters for different periods of the year and different ranges of wave heights highlighted an increase in wave height from 1970 to 2001 in summer (0.5 cm yr^{-1} for mean significant wave heights, and 2.6 cm yr^{-1} for the 5% highest significant wave heights at the Biscay buoy). Previous studies tend to show a regular increase or insignificant trends of wave height during the past few decades in that area. The examination of wave period and wave direction trends allowed for identifying a northerly shift of extreme wave direction during spring (13.2° from 1958 to 2001 for waves higher than the 90th percentiles at the Biscay buoy) and a southerly shift during autumn (−10.36° from 1974 to 2001 for waves higher than the 90th percentiles at the Biscay buoy).

In addition to the analysis of trends, the investigation of the interannual variability, using seasonal maps of normalized standard deviations, underlined large differences between seasons. Correlation maps between wave conditions and teleconnection pattern indices confirmed those seasonal differences. Moreover, they showed that correlation coefficients were constant from the open sea to the shore in the Bay of Biscay. Among the 10 leading teleconnection patterns of the Northern Hemisphere, the NAO and EA are predominant, impacting significant wave heights, mean periods, and peak directions during several seasons. At the Biscay buoy, the analysis of bivariate diagrams of correlation indicated that, during winter, energetic waves were strongly related to the NAO and EA indices. This is in agreement with previous studies. The fine spatial resolution used in the present study allowed for estimating the correlation of teleconnection patterns and wave characteristics in deep water as well as in intermediate water depths (about 20 m).

These results led to some coastal risk implications. Indeed, the summer wave height increase could lower beach accretion and induce a change in the beach morphological system. Moreover, the identified shifts in extreme wave directions during autumn and spring could induce important changes in the longshore sediment transport, with a potential impact on the coast morphology. The strong correlation between wave heights and the NAO, which is expected to be more often positive at the end of the twenty-first century, could induce more erosive events and thus strong variations in the sediment volume of sandy coasts.

The characterization of long-term trends and interannual variability of the present wave climate is a prerequisite for studying the present-day and future coastal response to variations in the context of climate change. The model and methods setup for the present study will be used to study the future wave climate using wind issued from global climate model projections.

Acknowledgments. This work was completed during a BRGM-CNRM doctorate program, funded by a Ph.D. grant from the AXA Research Fund, and codirected by P. Delecluse and D. Idier. The authors thank S. Caires and the anonymous reviewers for their careful read and constructive comments, which helped improve the manuscript. The authors also thank the ERA-40 team, M. Déqué and A. Braun (CNRM), CANDHIS, A. Le Berre and X. Kergadallan (CETMEF), and C. Deyts (CELM) for providing forcing and validation data; the Computing Center of Region Centre (CCSC) for providing access to the Phoebus computing system; and Grand Equipement National de Calcul Intensif (GENCI) for the access to the HPC resources of CINES under the allocation 2010-[c2010016403]. The authors gratefully acknowledge R. Magne (SHOM), F. Dupros, F. Boulahya, and N. Desramaut (BRGM) for their assistance, interesting exchanges, and ideas that led to improving this paper.

REFERENCES

Alves, J.-H. G. M., 2006: Numerical modeling of ocean swell contributions to the global wind-wave climate. *Ocean Modell.,* **11,** 98–122, doi:10.1016/j.ocemod.2004.11.007.

Ardhuin, F., and Coauthors, 2010: Semiempirical dissipation source functions for ocean waves. Part I: Definition, calibration, and validation. *J. Phys. Oceanogr.,* **40,** 1917–1941.

Bacon, S., and D. J. T. Carter, 1991: Wave climate changes in the North Atlantic and North Sea. *Int. J. Climatol.,* **11,** 545–558, doi:10.1002/joc.3370110507.

——, and ——, 1993: A connection between mean wave height and atmospheric pressure gradient in the North Atlantic. *Int. J. Climatol.,* **13,** 423–436, doi:10.1002/joc.3370130406.

Barnston, A. G., and E. L. Livezey, 1987: Classification, seasonality and persistence of low-frequency atmospheric circulation patterns. *Mon. Wea. Rev.,* **115,** 1083–1126.

Bengtsson, L., K. I. Hodges, and E. Roeckner, 2006: Storm tracks and climate change. *J. Climate,* **19,** 3518–3543.

Benoit, M., and F. Lafon, 2004: A nearshore wave atlas along the coasts of France based on the numerical modeling of wave climate over 25 years. *Waves,* J. McKee Smith, Ed., Vol. 1, *Coastal Engineering 2004: Proceedings of the 29th International Conference,* World Scientific Publishing, 714–726.

Caires, S., and A. Sterl, 2003: Validation of ocean wind and wave data using triple collocation. *J. Geophys. Res.,* **108,** 3098, doi:10.1029/2002JC001491.

——, ——, J.-R. Bidlot, N. Graham, and V. Swail, 2002: Climatological assessment of reanalysis ocean data. Preprints, *Seventh Int. Workshop on Wave Hindcasting and Forecasting,* Banff, AB, Canada, Meteorological Service of Canada, U.S. Army Engineer Research and Development Center, and Fleet Numerical Meteorology and Oceanography Center, 12 pp. [Available online at http://www.waveworkshop.org/7thWaves/Papers/Caires%20et%20al.pdf.]

——, V. R. Swail, and X. L. Wang, 2006: Projection and analysis of extreme wave climate. *J. Climate,* **19,** 5581–5605.

Cassou, C., 2008: Intraseasonal interaction between the Madden–Julian oscillation and the North Atlantic Oscillation. *Nature,* **455,** 523–527, doi:10.1038/nature07286.

Castelle, B., B. G. Ruessink, P. Bonneton, V. Marieu, N. Bruneau, and T. D. Price, 2010: Coupling mechanisms in double sandbar systems. Part 1: Patterns and physical explanation. *Earth Surf. Processes Landforms,* **35,** 476–486, doi:10.1002/esp.1929.

Dodet, G., X. Bertin, and R. Taborda, 2010: Wave climate variability in the north-east Atlantic Ocean over the last six decades. *Ocean Modell.,* **31,** 120–131, doi:10.1016/j.ocemod.2009.10.010.

Dupuis, H., D. Michel, and A. Sottolichio, 2006: Wave climate evolution in the Bay of Biscay over two decades. *J. Mar. Syst.,* **63,** 105–114, doi:10.1016/j.jmarsys.2006.05.009.

Grabemann, I., and R. Weisse, 2008: Climate change impact on extreme wave conditions in the North Sea: An ensemble study. *Ocean Dyn.,* **58,** 199–212, doi:10.1007/s10236-008-0141-x.

Hurrell, J. W., Y. Kushnir, G. Ottersen, and M. Visbeck, 2003: An overview of the North Atlantic Oscillation. *The North Atlantic Oscillation: Climatic Significance and Environmental Impact, Geophys. Monogr.,* Vol. 134, Amer. Geophys. Union, 1–35.

Izaguirre, C., F. J. Méndez, M. Menéndez, and I. J. Losada, 2011: Global extreme wave height variability based on satellite data. *Geophys. Res. Lett.,* **38,** L10607, doi:10.1029/2011GL047302.

Kalnay, E., and Coauthors, 1996: The NCEP/NCAR 40-Year Reanalysis Project. *Bull. Amer. Meteor. Soc.,* **77,** 437–471.

Komen, G. J., L. Cavaleri, M. Donelan, K. Hasselmann, S. Hasselmann, and P. A. E. M. Janssen, 1994: *Dynamics and Modelling of Ocean Waves*. Cambridge University Press, 556 pp.

Kushnir, Y., V. J. Cardone, J. G. Greenwood, and M. A. Cane, 1997: The recent increase in North Atlantic wave heights. *J. Climate,* **10,** 2107–2113.

Le Cozannet, G., S. Lecacheux, E. Delvallée, N. Desramaut, C. Oliveros, and R. Pedreros, 2011: Teleconnection pattern influence on sea-wave climate in the Bay of Biscay. *J. Climate,* **24,** 641–652.

Magne, R., F. Ardhuin, and A. Roland, 2010: Waves forecast and hincast from global ocean to the beach. *Eur. J. Environ. Civil Eng.,* **14,** 149–162.

NGDC, cited 2009: 2-Minute gridded global relief data (ETOPO2v2). [Available online at http://www.ngdc.noaa.gov/mgg/fliers/06mgg01.html.]

Nicholls, R. J., P. P. Wong, V. R. Burkett, J. O. Codignotto, J. E. Hay, R. F. McLean, S. Ragoonaden, and C. D. Woodroffe, 2007: Coastal systems and low-lying areas. *Climate Change 2007: Impacts, Adaptation and Vulnerability,* M. L. Parry et al., Eds., Cambridge University Press, 315–356.

Parisot, J. P., S. Capo, D. Rihouey, H. Howa, F. Desmazes, and L. Fauque, 2010: Analyse de l'évolution morphodynamique de la plage du Truc Vert (Gironde) sur une période décennale. *Proc. XIèmes Journées Nationales Génie Côtier*-Génie Civil, Les Sables d'Olonne, France, Editions PARALIA and Centre Français du Littoral, 387–396.

Pierson, W. J., and L. Moskowitz, 1964: A proposed spectral form for fully developed wind seas based on the similarity theory of S. A. Kitaigorodskii. *J. Geophys. Res.,* **69,** 5181–5190.

Ranasinghe, R., R. McLoughlin, A. Short, and G. Symonds, 2004: The Southern Oscillation index, wave climate, and beach rotation. *Mar. Geol.,* **204,** 273–287, doi:10.1016/S0025-3227(04)00002-7.

Seierstad, I. A., D. B. Stephenson, and N. G. Kvamstø, 2007: How useful are teleconnection patterns for explaining variability in extratropical storminess? *Tellus,* **59A,** 170–181, doi:10.1111/j.1600-0870.2007.00226.x.

Small, C., and R. J. Nicholls, 2003: A global analysis of human settlement in coastal zones. *J. Coast. Res.,* **19,** 584–599.

Student, 1908: The probable error of a mean. *Biometrika,* **6,** 1–25, doi:10.1093/biomet/6.1.1.

Terray, L., M. E. Demory, M. Déqué, G. D. Coetlogon, and E. Maisonnave, 2004: Simulation of late-twenty-first-century changes in wintertime atmospheric circulation over Europe due to anthropogenic causes. *J. Climate,* **17,** 4630–4635.

Tolman, H. L., 2009: User manual and system documentation of WAVEWATCH III version 3.14. NOAA/NWS/NCEP/MMAB Tech. Note 276, 194 pp.

Uppala, S. M., and Coauthors, 2005: The ERA-40 Re-Analysis. *Quart. J. Roy. Meteor. Soc.,* **131,** 2961–3012, doi:10.1256/qj.04.176.

Wang, X. L., and V. R. Swail, 2001: Changes of extreme wave heights in Northern Hemisphere oceans and related atmospheric circulation regimes. *J. Climate,* **14,** 2204–2221.

——, and ——, 2002: Trends of Atlantic wave extremes as simulated in a 40-yr wave hindcast using kinematically reanalyzed wind fields. *J. Climate,* **15,** 1020–1035.

——, and ——, 2006: Climate change signal and uncertainty in projections of ocean wave heights. *Climate Dyn.,* **26,** 109–126, doi:10.1007/s00382-005-0080-x.

——, F. W. Zwiers, and V. R. Swail, 2004: North Atlantic Ocean wave climate change scenarios for the twenty-first century. *J. Climate,* **17,** 2368–2383.

Woolf, D. K., P. G. Challenor, and P. D. Cotton, 2002: Variability and predictability of the North Atlantic wave climate. *J. Geophys. Res.,* **107,** 3145, doi:10.1029/2001JC001124.

Yin, J. H., 2005: A consistent poleward shift of the storm tracks in simulations of 21st century climate. *Geophys. Res. Lett.,* **32,** L18701, doi:10.1029/2005GL023684.

Žagar, N., M. Žagar, J. Cedilnik, G. Gregorič, and J. Rakovec, 2006: Validation of mesoscale low-level winds obtained by dynamical downscaling of ERA40 over complex terrain. *Tellus,* **58A,** 445–455, doi:10.1111/j.1600-0870.2006.00186.x.

Zijderveld, A., and M. Verlaan, 2004: Towards a new gridded bathymetry for storm surge forecasting in the North Sea. *Geophysical Research Abstracts,* Vol. 6, Abstract 05177. [Available online at http://www.cosis.net/abstracts/EGU04/05177/EGU04-J-05177.pdf.]